NASA Technical Memorandum 100560

APPLICATION OF A NONISENTROPIC FULL POTENTIAL METHOD TO AGARD STANDARD AIRFOILS

WOODROW WHITLOW, JR.

JANUARY 1988

NASA

National Aeronautics and
Space Administration

Langley Research Center
Hampton, Virginia 23665-5225

APPLICATION OF A NONISENTROPIC FULL POTENTIAL METHOD TO AGARD STANDARD AIRFOILS

Woodrow Whitlow, Jr.*
NASA Langley Research Center
Hampton, Virginia 23665-5225

Abstract

An entropy-correction method for the unsteady full potential equation is presented. The unsteady potential equation is modified to model the entropy jumps across shock waves. The conservative form of the modified equation is solved in generalized coordinates using an implicit, approximate factorization method. A flux-biasing differencing method, which generates the proper amounts of artificial viscosity in supersonic regions, is used to discretize the flow equations in space. Calculated results are presented for the NLR 7301, NACA 0012, and NACA 64A010A airfoils. Comparisons of the present method and solutions of the Euler equations are presented for the NLR 7301 airfoil, and comparisons of the present method and experimental data are presented for all three airfoils. The comparisons show that the present method more accurately models solutions of the Euler equations and experiment than does the isentropic potential formulation. In addition, it is shown that modeling shock-generated entropy extends the range of validity of the full potential method.

Nomenclature

a	speed of sound
A_1, A_2, A_3	metrics of coordinate transformation, Equation (7)
c	airfoil chord
C_p	pressure coefficient
$\tilde{C}_p$	first harmonic of pressure coefficient
ΔC_p	first harmonic of lifting pressure
h	computational time step
i, j	indices of grid points
I	identity matrix
J	Jacobian of coordinate transformation
k	reduced frequency based on semichord
M	Mach number
q	total velocity
R	gas constant
Δs	entropy change
t	physical time
U, W	contravariant velocities, Equation (6)
x, z	physical coordinate directions
α	angle of attack
α_o	oscillation angle
β	$\dfrac{\rho^{2-\gamma}}{J}$
γ	ratio of specific heats
Γ	change in potential across the wake
δ	difference operator
ξ, ζ	computational coordinate directions
ρ	density
$\bar{\rho}$	ρ/J
$\tilde{\rho}$	biased density

---

*Research Scientist, Loads and Aeroelasticity Division, Unsteady Aerodynamics Branch, Member AIAA.

τ	computational time
ϕ	velocity potential
$<>$	average of quantity across the wake

Subscripts

i	isentropic
n	normal to shock wave
∞	free stream conditions

Superscripts

l	lower side of wake
n	computational time level
u	upper side of wake
*	sonic conditions

Introduction

Modern aircraft typically operate at high speeds where aeroelastic instabilities are more likely to occur. To successfully predict and analyze such aeroelastic phenomena, the aircraft designer needs methods that accurately predict the aerodynamic loads that the vehicle experiences. Since many critical aeroelastic phenomena occur at transonic speeds, methods based on linear aerodynamic theory cannot accurately predict these aeroelastic responses. Thus, it is necessary to use an aerodynamic method that can predict time-accurate solutions of nonlinear flows and that can accurately model shock waves and their unsteady motions.

When shock waves appear in transonic flow fields, aerodynamic loads predicted using potential flow theory can be highly inaccurate and even multivalued. Multiple solutions of the potential equation were first observed in two dimensions by Steinhoff and Jameson [1]. Salas and Gumbert [2] showed that the phenomenon is not confined to a particular airfoil or flow condition. Williams et al. [3] calculated multiple solutions using two-dimensional (2-D) transonic small disturbance (TSD) theory, and Gibbons et al. [4] extended Williams' results to three dimensions and showed multiple TSD solutions for high-aspect-ratio wings. For lower-aspect-ratio wings, multiple solutions were not observed, but calculated lift coefficients were highly inaccurate when shock waves were present in the flow field.

Since potential theory can yield inaccurate transonic aerodynamic loads, aeroelastic analysis performed using these loads has to be considered unreliable. One reason for this inaccuracy is that potential theory does not model the entropy change that a fluid particle experiences as it passes through shock waves. As a result, calculated shock waves can have the wrong strength and the wrong location.

The most widely used methods for unsteady, nonlinear flow analysis are based on TSD theory [5-7]. Fuglsang and Williams [8] modeled the effects of entropy jumps through shock waves in 2-D TSD theory. Gibbons et al. [4] extended that method to three dimensions. These efforts resulted in

TSD methods that more closely model solutions of the Euler equations than does isentropic TSD theory.

Whitlow et al. [9] developed a full potential method for predicting unsteady aerodynamic loads on 2-D bodies when nonisentropic effects are important. The nonisentropic effects of embedded shock waves were modeled by modifying the isentropic density to include the effects of shock-generated entropy. This yielded potential flow solutions that more accurately model Euler solutions. This method is an extension of the Hafez-Lovell method for steady full potential flows [10].

In the present effort, the nonisentropic full potential method of Whitlow et al. is implemented in a computer code and applied to AGARD standard airfoils for validation. A flux-biasing differencing method [11,12] is used to discretize the flow equations and to capture shock discontinuities. To increase computational efficiency, grids for unsteady calculations are generated, at each time step, using linear interpolation between grids calculated at extreme airfoil positions. The present method allows accurate predictions of unsteady aerodynamic loads at relatively low computational expense and alleviates the problem of multiple potential flow solutions [9]. In this paper, comparisons of computed results with Euler calculations and with experimental data are presented. These comparisons show that more accurate modeling of flow fields is achieved with the present method than with an isentropic potential method. The comparisons also illustrate how the range of validity of potential flow theory is extended when the nonisentropic effects of shock waves are modeled.

Problem Formulation

Governing Equations

The formulation used in the present effort is that presented by Bridgeman et al. [13]. The flow field is described by the two-dimensional, unsteady full potential equation in conservation form

$$\rho_t + (\rho\phi_x)_x + (\rho\phi_z)_z = 0 \tag{1}$$

where ϕ is the velocity potential, and the density ρ is determined from Bernoulli's equation

$$\rho = [1 + \frac{\gamma-1}{2}(M_\infty^2 - 2\phi_t - \phi_x^2 - \phi_x^2)]^{\frac{1}{\gamma-1}} \tag{2}$$

The spatial coordinates, x and z, are normalized by airfoil chord c, and time t is normalized by a_∞/c, where a_∞ is the free stream speed of sound. Density is normalized by the free stream density ρ_∞, and ϕ is normalized by $a_\infty c$. In (2), M_∞ represents the free stream Mach number.

In this effort, all calculations are performed in a coordinate system that conforms to the airfoil contour. The transformation to a body-fitted coordinate system is given by

$$\xi = \xi(x,z,t)$$

$$\zeta = \zeta(x,z,t) \tag{3}$$

$$\tau = t$$

where ξ and ζ are the computational coordinate directions around and normal to the airfoil, as shown in figure 1, and τ is the computational time. The strong conservation form of (1) is maintained by writing the continuity equation in transformed coordinates as

$$(\frac{\rho}{J})_\tau + (\frac{\rho U}{J})_\xi + (\frac{\rho W}{J})_\zeta = 0 \tag{4}$$

Equation (2) transforms to

$$\rho = \{1 + \frac{\gamma-1}{2}[M_\infty^2 - 2\phi_\tau - (U + \xi_t)\phi_\xi$$
$$- (W + \zeta_t)\phi_\zeta]\}^{\frac{1}{\gamma-1}} \tag{5}$$

where the contravariant velocities in the ξ and ζ directions, U and W, respectively, are given by

$$U = \xi_t + A_1\phi_\xi + A_2\phi_\zeta$$

$$\tag{6}$$

$$W = \zeta_t + A_2\phi_\xi + A_3\phi_\zeta$$

The metric terms, A_1, A_2, and A_3, are related to the computational coordinate directions by

$$A_1 = \xi_x^2 + \xi_z^2$$

$$A_2 = \xi_x\zeta_x + \xi_z\zeta_z \tag{7}$$

$$A_3 = \zeta_x^2 + \zeta_z^2$$

The Jacobian of the transformation J is

$$J = \xi_x\zeta_z - \xi_z\zeta_x \tag{8}$$

Approximate Factorization

Equation (4) is solved using first order backward differencing in time and second order central differencing in space. The time derivative of density is linearized about previous time levels such that conservation form is maintained. The resulting equation is factored into the form $L_\xi L_\zeta \Delta\phi = F$. This becomes

$$[I + hU^n\delta_\xi - \frac{h^2}{\beta^n}\delta_\xi(\bar{\rho}A_1)^n\delta_\xi]$$

$$\times [I + hW^n\delta_\zeta - \frac{h^2}{\beta^n}\delta_\zeta(\bar{\rho}A_3)^n\delta_\zeta](\phi^{n+1} - \phi^n)$$

$$= (\phi^n - \phi^{n-1}) + \frac{\beta^{n-1}}{\beta^n}(\phi^n - 2\phi^{n-1} + \phi^{n-2})$$

$$+ \frac{h}{\beta^n}(\bar{\rho}^n - \bar{\rho}^{n-1}) \qquad (9)$$

$$+ h\frac{\beta^{n-1}}{\beta^n}(U^{n-1}\delta_\xi + W^{n-1}\delta_\zeta)(\phi^n - \phi^{n-1})$$

$$+ \frac{h^2}{\beta^n}[\delta_\xi(\frac{\overset{\wedge}{\rho}U}{J})^n + \delta_\zeta(\bar{\rho}W)^n - F_\infty]$$

where

$$L_\xi = [I + hU^n\delta_\xi - \frac{h^2}{\beta^n}\delta_\xi(\bar{\rho}A_1)^n\delta_\xi]$$

$$L_\zeta = [I + hW^n\delta_\zeta - \frac{h^2}{\beta^n}\delta_\zeta(\bar{\rho}A_3)^n\delta_\zeta]$$

$$\Delta\phi = \phi^{n+1} - \phi^n$$

In (9), δ_ξ and δ_ζ represent central difference operators, the superscripts n, n-1, and n+1 represent computational time levels,

$$h = \Delta\tau$$

$$\bar{\rho} = \frac{\rho}{J}$$

$$\beta = \rho\frac{2-\gamma}{J}$$

The density biased in the ξ direction is denoted by $\overset{\wedge}{\rho}$, and F_∞ is a correction to the residual due to incomplete metric cancellation [13,14]

Airfoil Boundary Conditions

The condition that the flow be tangent to the airfoil is satisfied by requiring that the contravariant velocity in the ζ direction vanish at the airfoil boundary. The flow tangency condition is expressed

$$W = \zeta_t + A_2\phi_\xi + A_3\phi_\zeta = 0 \qquad (10)$$

and is applied by writing ϕ_ζ at the airfoil as

$$(\phi_\zeta)_{i,J} = -(\frac{A_2}{A_3}\phi_\xi)_{i,J} - (\frac{\zeta_t}{A_3})_{i,J} \qquad (11)$$

where the subscript J represents points on the body. The tangency condition implies that

$$(\bar{\rho}W)_{i,J-1/2} = -(\bar{\rho}W)_{i,J+1/2} \qquad (12)$$

The subscript J-1/2 represents points inside the airfoil. Using (11) and (12), the flow tangency condition is imposed implicitly on both sides of (9) by changing the L_ξ and L_ζ operators to

$$L_\xi = [I + hU^n\delta_\xi - \frac{h^2}{\beta^n}\delta_\xi\bar{\rho}^n(A_1 - \frac{A_2^2}{A_3})^n\delta_\xi]$$

$$L_\zeta = [I - \frac{2h^2}{\beta^n}((\bar{\rho}A_3)^n\delta_\zeta)_{i,J+1/2}]$$

and by representing the $\delta_\zeta(\bar{\rho}W)_{i,J}$ term on the right side as $2(\bar{\rho}W)_{i,J+1/2}$.

To apply the flow tangency at the instantaneous surface position of moving bodies requires a new grid at each time step. In this effort, the computational grids were generated using an elliptic grid generation method [15]. Since the resources needed to compute the necessary grids using an elliptic method can exceed those necessary for the aerodynamic calculations, an efficient interpolation method is used to generate the required grids. To simulate the unsteady motion, grids are calculated at the extreme airfoil positions, and grids for all other positions are determined using linear interpolation. Interior grid points are redistributed at each time step, while points on the outer boundary remain fixed. Details of this method are given in reference 9.

Unsteady Wake Condition

For lifting flows, the shed vorticity is represented as a jump in potential across a wake line. For isentropic flows, the following wake boundary condition [13] is used

$$\Gamma_\tau + <W>\Gamma_\zeta = 0 \qquad (13)$$

where Γ is the jump in potential across the wake, $\phi^u - \phi^l$, and $<W>$ is the average of W above and below the wake, $1/2(W^u + W^l)$. The unsteady transport condition for the jump in potential, (13), is obtained by assuming that the isentropic density and normal velocity are continuous across the wake. It does not model the jump in entropy across the wake that results when shock waves of different strengths are on the upper and lower surfaces.

Far-Field Conditions

In the far field, the flow is set to free stream conditions

$$\phi = M_\infty x$$

$$\rho = 1$$

Flux Biasing

The spatial terms on the right side of (9) that make up the residual are centrally differenced about the node point (i,j) to give

$$\delta_\xi (\frac{\overset{\sim}{\rho U}}{J})_{i,j} = (\frac{\overset{\sim}{\rho U}}{J})_{i+1/2,j} - (\frac{\overset{\sim}{\rho U}}{J})_{i-1/2,j}$$

$$\delta_\zeta (\overline{\rho W})_{i,j} = (\overline{\rho W})_{i,j+1/2} - (\overline{\rho W})_{i,j-1/2}$$

The computational cell is shown in figure 2. In supersonic regions, artificial viscosity, necessary to capture shocks, is introduced by biasing the density in the upwind direction. Although it is generally necessary to bias the density in both computational directions, in this work, biasing only in the ξ direction has been found to be satisfactory. The biased density $\overset{\sim}{\rho}$ is defined as (for U > 0)

$$\overset{\sim}{\rho}_{i+1/2,j} = \frac{1}{q_{i+1/2,j}}[\rho q - \Delta\xi(\rho q)_\xi^-]_{i+1/2,j}$$

$$= \frac{1}{q_{i+1/2,j}}[(\rho q)_{i+1/2,j} - (\rho q)_{i+1/2,j}^- \qquad (14)$$

$$+ (\rho q)_{i-1/2,j}^-]$$

where

$$(\rho q)^- = \rho q - \rho^* q^* \qquad q > q^*$$
$$\qquad\qquad\qquad\qquad (15)$$
$$0 \qquad\qquad q \le q^*$$

q is the flow speed, $q = (A_1 \phi_\xi^2 + 2 A_2 \phi_\xi \phi_\zeta + A_3 \phi_\zeta^2)^{1/2}$, and q^* and ρ^* are the sonic speed and density, respectively, given by

$$q^{*2} = \frac{2}{\gamma+1}[1 + \frac{\gamma-1}{2}(M_\infty^2 - 2\phi_\tau - 2\xi_t\phi_\xi - 2\zeta_t\phi_\zeta)] \qquad (16)$$

$$\rho^* = (q^{*2})^{\frac{1}{\gamma-1}} \qquad (17)$$

For steady flows, ρ^* and q^* are constants that are computed once. For unsteady flows, ρ^* and q^* must be computed at each grid point at every time step.

Flux biasing (a) accurately tracks sonic conditions and requires no empirical constants to specify the amount of aritifical viscosity (b) produces no velocity overshoots at shock waves, allowing for larger time steps--increasing computational efficiency--for unsteady calculations, (c) produces well defined, monotone shock profiles with a maximum two point transition between the upstream and downstream states, and (d) dissipates expansion shock waves, ruling out solutions with such nonphysical characteristics.

Entropy-Correction Method

When a fluid particle passes through a shock wave, it experiences a change in entropy Δs which is a function of the upstream Mach number normal to the shock M_n

$$\frac{\Delta s}{R} = \frac{1}{\gamma-1}\{1n(\frac{2\gamma}{\gamma+1}M_n^2 - \frac{\gamma-1}{\gamma+1}) - \gamma 1n[\frac{(\gamma+1)M_n^2}{(\gamma-1)M_n^2+2}]\} \qquad (18)$$

For unsteady flows, the shock speed must be monitored to obtain the Mach number relative to the shock. Here, the entire shock is assumed to move at the same speed as the base of the shock. The nonisentropic density is

$$\rho = \rho_i e^{\frac{-\Delta s}{R}} \qquad (19)$$

which substituted into the continuity equation, (1), yields

$$(\rho_i e^{\frac{-\Delta s}{R}})_t + (\rho_i e^{\frac{-\Delta s}{R}}\phi_x)_x + (\rho_i e^{\frac{-\Delta s}{R}}\phi_z)_z = 0 \qquad (20)$$

Details for modeling the shock-generated entropy are given below. Equation (4) is discretized as

$$\frac{\bar{\rho}_{i,j}^{n+1} - \bar{\rho}_{i,j}^{n}}{h} + (\frac{\overset{\sim}{\rho U}}{J})_{i+1/2,j}^{n+1} - (\frac{\overset{\sim}{\rho U}}{J})_{i-1/2,j}^{n+1}$$

$$\tag{21}$$

$$+ (\overline{\rho W})_{i,j+1/2}^{n+1} - (\overline{\rho W})_{i,j-1/2}^{n+1} = 0$$

Downstream of shock waves, (21) becomes

$$[(\overline{\rho_i e^{\frac{-\Delta s}{R}}})_{i,j}^{n+1} - (\overline{\rho_i e^{\frac{-\Delta s}{R}}})_{i,j}^{n}]\frac{1}{h}$$

$$+ (\frac{\overset{\sim}{\rho U}}{J})_{i+1/2,j}^{n+1} - (\frac{\overset{\sim}{\rho U}}{J})_{i-1/2,j}^{n+1} \tag{22}$$

$$+ (\overline{\rho_i e^{\frac{-\Delta s}{R}} W})_{i,j+1/2}^{n+1} - (\overline{\rho_i e^{\frac{-\Delta s}{R}} W})_{i,j-1/2}^{n+1} = 0$$

where Δs is a function of $\quad M_{n_{i-3/2,j}}$,

$$\overset{\sim}{\rho}_{i+1/2,j} = \frac{1}{q_{i+1/2,j}} [(\rho_i e^{\frac{-\Delta s}{R}} q)_{i+1/2,j}$$

$$- (\rho q)_{i+1/2,j}^{-} + (\rho q)_{i+1/2,j}^{-}] \tag{23}$$

$$(\rho q)^{-} = \rho_i e^{\frac{-\Delta s}{R}} q - \rho^* q^* \qquad q > q^*$$

$$0 \qquad\qquad q \le q^*$$

At shock points,

$$\overset{\sim}{\rho}_{i+1/2,j} = (\rho_i e^{\frac{-\Delta s}{R}})_{i+1/2,j} +$$

$$\frac{1}{q_{i+1/2,j}}(\rho_i q - \rho^* q^*)_{i-1/2,j}$$

The computational cell at shock points is shown in figure 3.

In the approximate factorization scheme, the entropy-correction method is implemented by representing the

$$\frac{h}{\beta_n}(\overline{\rho}^n - \overline{\rho}^{n-1}) \text{ and } \frac{h^2}{\beta_n}[\delta_\xi(\frac{\overset{\sim}{\rho U}}{J})^n + \delta_\zeta (\overline{\rho W})^n]$$

terms in (9) as

$$\frac{h}{\beta_n}[(\overline{\rho_i e^{\frac{-\Delta s}{R}}})_{i,j}^n - (\overline{\rho_i e^{\frac{-\Delta s}{R}}})_{i,j}^{n-1}] \text{ and }$$

$$\frac{h^2}{\beta_n}[(\frac{\overset{\sim}{\rho U}}{J})_{i+1/2,j}^n - (\frac{\overset{\sim}{\rho U}}{J})_{i-1/2,j}^n$$

$$+ (\overline{\rho_i e^{\frac{-\Delta s}{R}} W})_{i,j+1/2}^n - (\overline{\rho_i e^{\frac{-\Delta s}{R}} W})_{i,j-1/2}^n],$$

respectively, where $\overset{\sim}{\rho}_{i+1/2,j}$ is given by (23). The effect of the entropy corrections is to introduce a source distribution along the shock. The source strength is dependent upon Δs.

The nonisentropic wake condition is determined by requiring that the pressure and normal velocity be continuous across the wake. The nonisentropic pressure coefficient is given by

$$C_p = \frac{2}{\gamma M_\infty^2} [(\rho_i e^{\frac{-\Delta s}{R}})^\gamma - 1]$$

and the zero pressure jump condition is enforced by requiring that

$$(\rho_i e^{\frac{-\Delta S}{R}})^u = (\rho_i e^{\frac{-\Delta S}{R}})^l$$

This yields the following condition for the jump in the potential

$$\Gamma_\tau + <W> \Gamma_\zeta = [(e^{\frac{-\Delta s}{R}})^u - (e^{\frac{-\Delta s}{R}})^l]$$

$$- \frac{1}{\gamma-1}[(\rho_i^{\gamma-1} - 1)^u (\frac{\Delta s}{R})^u - (\rho_i^{\gamma-1} - 1)^l (\frac{\Delta s}{R})^l]$$

For flows with no shocks and hence no entropy production, this reduces to the isentropic wake condition (13).

Results and Discussions

To assess the present method, pressures were calculated for the NLR 7301, NACA 0012, and NACA 64A010A airfoils using the isentropic and nonisentropic methods. Steady pressures on the NLR 7301 airfoil were calculated at its design conditions and at a transonic high lift condition. Comparisons of the full potential calculations with

5

experimental data [16] and with Euler calculations are presented. Unsteady pressures on the NACA 0012 oscillating in pitch about its quarter chord were computed and comparisons made with experimental data [17]. Finally, calculated unsteady pressures for the NACA 64A010A oscillating in pitch about its quarter chord are compared with experimental data [18]. The unsteady pressures were calculated using 600 time steps per cycle of motion. Modeling nonisentropic effects increases the cost of the computations by 35-40 percent.

NLR 7301

In this section, calculations made for the NLR 7301 airfoil are presented. The full potential calculations are compared with Euler calculations and with experiment. Steady pressures on the NLR 7301 at its design conditions, $M_\infty = 0.721$ and $\alpha = -0.19°$, are shown in figure 4. Included are full potential calculations, Euler calculations [19] and experimental data. The isentropic and nonisentropic potential calculations are shown as one line, since, for this case, the effects or shock-generated entropy are small, and the two potential solutions are nearly identical. The results from the present method show very good agreement with experimental data and with the Euler results. The shock location calculated with the present method is slightly upstream of the experimental location and slightly downstream of the location predicted by the Euler solution.

The potential flow calculations shown in figure 4 illustrate the importance of properly constructing body-fitted grids for numerical calculations. Due to changes in the grid construction, these calculations are a significant improvement upon similar results presented in reference 9. Figure 5 shows calculated pressures for the NLR 7301 as presented in reference 9. The only difference in figures 4 and 5 is the grid used in the full potential calculations. The trailing edge region of the original grid used for the potential calculations in figure 5 is shown in figure 6. Near the trailing edge, the grid lines in the wake are highly skewed, resulting in inaccurate metric coefficients. This causes the circulation and the calculated pressures to be in error. Figure 7 shows the trailing edge region of the grid used in the present calculations. This grid is not skewed in the trailing edge region, and, as a result, the calculations are much more accurate.

A comparison of isentropic potential calculations and Euler calculations is shown in figure 8 for $M_\infty = 0.7$, $\alpha = 2°$. The shock calculated with the isentropic potential method is much too strong and too far aft on the airfoil, suggesting that this case is outside the range of validity of isentropic potential theory. Figure 9 shows a comparison of nonisentropic potential calculations with Euler calculations for the case of figure 8. Modeling the nonisentropic effects brings the potential flow solution into good agreement with the Euler results. The shock waves differ by 4-5 percent of chord in location and have nearly the same strength. In addition, the agreement of the nonisentropic potential solution and the Euler solution is excellent on the lower surface of the airfoil.

NACA 0012

In this section, the calculations for the NACA 0012 airfoil are presented. Isentropic and nonisentropic unsteady pressures are computed for the airfoil pitching about its quarter chord location, $\alpha(\tau) = 0.016° + 2.51° \sin (k\tau)$, at $M_\infty = 0.755$ and $k = 0.0814$. Comparisons of the isentropic and nonisentropic steady solutions and comparisons of the first harmonic of the unsteady pressures, normalized by the amplitude of oscillation, with experimental data (Reynolds number $= 5.5 \times 10^6$) are presented. Fourier analysis of the time-dependent data presented in reference 16 is used to obtain the first harmonics of the experimental pressures. First harmonics of the calculated pressures are obtained by calculating the flow field for four cycles of the unsteady motion and performing Fourier analysis of the data for the last cycle of motion.

Calculated isentropic and nonisentropic steady pressures are shown in figure 10. For this case, the solution contains a weak shock, and the effects of the entropy corrections on the steady solution are minimal. Comparisons of the mean pressures over a cycle of motion are shown in figure 11. Figure 11(a) shows the pressures on the airfoil upper surface, and those on the lower surface are shown in figure 11(b). For both surfaces, agreement between the calculations and experiment is very good. Modeling the shock-generated entropy causes a slight forward shift in the mean shock position, and downstream of the shock wave, the level of the pressures is changed to be in better agreement with the measured data.

Comparisons of the first harmonic of unsteady pressures are shown in figure 12. Pressures on the upper surface are shown in figure 12(a). The real part of the calculations show good agreement with experiment, with the imaginary component of the pressures indicating a calculated shock wave that is stronger than and aft of the measured shock. This can be expected for comparisons of inviscid calculations with data measured at a relatively low Reynolds number. The TSD calculations, coupled with a viscous boundary layer model, presented by Howlett and Bland [20] indicate that viscous effects are significant for this case. The nonisentropic calculations show a slight weakening and forward shift of the shock wave toward the measured location. Figure 12(b) shows the pressures on the lower surface. The real part of the calculated solutions shows very good agreement with the measured data, while the imaginary part indicates a shock that is too strong and aft of the measured location. The real part of the nonisentropic calculations indicate weakening of the shock wave and an upstream shift in its location, whereas the imaginary component shows minimal effects on the shock strength and location.

NACA 64A010A

In this section, calculations for the NACA 64A010A airfoil are presented. The airfoil is the model of the NACA 64A010 airfoil tested at the NASA Ames Research Center [18]. That model has a small amount of camber and surface waviness. The comparisons presented here are for test conditions at $M_\infty = 0.796$ and Reynolds number of 12.5×10^6.

Figure 13 shows the measured and calculated steady pressures on the airfoil surface. The surface waviness is evident in the pressure distributions upstream of the airfoil midchord. Agreement between the calculations and experiment is good, with the level of the calculated pressures upstream of the shock slightly higher than those

measured during the experiment. On the forward portion of the airfoil, the isentropic and nonisentropic pressures are nearly the same, and no differences in the plotted pressures are evident. The calculated shock wave is 2-3 percent of chord downstream of the measured location. It is of moderate strength, and the effects of the nonisentropic corrections is to cause a slight weakening and forward shift of the shock. The differences between the measured and calculated pressures are as expected for comparison of an inviscid method with experimental data. TSD calculations shown in reference [20] indicate that modeling viscous effects would improve the comparisons with experiment.

Unsteady pressures were calculated for the airfoil oscillating in pitch about its quarter chord, $\alpha(\tau) = \alpha_0 \sin(k\tau)$. Figure 14 shows the first harmonic of the unsteady pressures for $\alpha_0 = 1.02°$, $k = 0.051$. Except in the vicinity of the shock wave, the agreement between calculations and experiment is good, with the better agreement shown with the imaginary component of the pressures. The calculated shock wave is downstream of the experimental location and is stronger than the measured shock. For this case, the general effect of the entropy corrections is to cause a slight shift forward and decrease in the amplitude of the shock pulse. On the upper surface, the imaginary part of the nonisentropic shock pulse shows a slight increase in amplitude.

Figure 15 shows the unsteady pressures for $\alpha_0 = 1.02°$, $k = 0.101$. For this higher frequency case, the differences in the isentropic and nonisentropic calculations are more pronounced. The agreement between the calculations and experiment is good, except in the vicinity of the shock pulse, with the imaginary components showing the better agreement. The effect of the entropy corrections is to decrease the amplitude and width of the imaginary part of shock pulse and to increase the amplitude of the real part of the shock pulse. These effects of the nonisentropic corrections result in improved agreement of the calculations with the experimental data.

Figure 16 shows the unsteady pressures for $\alpha_0 = 2°$, $k = 0.101$. Except for the shock pulse being downstream of the measured location, the agreement between the nonisentropic calculations and experiment is good. Modeling the nonisentropic effects causes an increase in the amplitude of the real part of the shock pulse and a decrease in the imaginary part. For both components of the first harmonic of the pressures, the effects of the nonisentropic corrections result in improved agreement of the calculations with experiment.

Concluding Remarks

A method for modeling the effects of shock-generated entropy has been developed for the unsteady full potential equation. This was accomplished by modifying the isentropic density downstream of shock waves to account for the local change in entropy. The resulting method was tested for flow past the NLR 7301, NACA 0012, and NACA 64A010A airfoils. Comparisons of the present method with experimental data and Euler calculations were made for the NLR 7301 airfoil, and comparisons of the present method were made with experiment for the NACA 0012 and NACA 64A010A airfoils.

Calculations for the NACA 0012 and NACA 64A010A

airfoils indicate that for shock waves of weak to moderate strength, modeling the nonisentropic effects has small effects on the steady state pressures--slight weakening and forward shift of the computed shock wave. For the NACA 0012 airfoil, modeling the nonisentropic effects cause weakening of and a small forward shift in the shock pulse. Calculations on the NACA 64A010A show that modeling the unsteady shock-generated entropy causes a forward shift in the location of the shock pulse, but for some cases, the amplitude of the pulse is increased. In those cases, agreement with experimental data is improved. The calculations for the NACA 64A010A show that although the nonisentropic effects on the steady solution are small, the effects on the unsteady solution can be significant.

A strong shock case for the NLR 7301 shows that modeling nonisentropic effects can extend the range of validity of potential flow methods. Accurate solutions can be obtained at conditions for which isentropic potential yields highly inaccurate solutions.

References

[1] J. Steinhoff and A. Jameson 1982 Multiple Solutions of the Transonic Potential Flow Equation. AIAA Journal Vol. 20 1521-1525.

[2] M. D. Salas and C. R. Gumbert 1985 Breakdown of the Conservative Potential Equation. AIAA Paper 85-0367.

[3] M. Williams, S. Bland and J. Edwards 1985 Flow Instabilities in Transonic Small Disturbance Theory. AIAA Journal Vol. 23 1491-1496.

[4] M. D. Gibbons, W. Whitlow, Jr. and M. H. Williams 1986 Nonisentropic Unsteady Three Dimensional Small Disturbance Potential Theory. AIAA Paper 86-0863.

[5] W. F. Ballhaus and P. M. Goorjian 1977 Implicit Finite-Difference Computations of Unsteady Transonic Flows about Airfoils. AIAA Journal Vol. 15 1728-1735.

[6] W. Whitlow, Jr. 1983 XTRAN2L: A Program for Solving the General-Frequency Unsteady Transonic Small Disturbance Equation. NASA TM 85723.

[7] C. J. Borland and D. P. Rizzetta 1982 Transonic Unsteady Aerodynamics for Aeroelastic Applications. AFWAL TR 80-3107, Vol. I--Technical Development Summary.

[8] D. F. Fugisang and M. H. Williams 1985 Non-Isentropic Unsteady Transonic Small Disturbance Theory. AIAA Paper 85-0600.

[9] W. Whitlow, Jr., M. M. Hafez and S. J. Osher 1986 An Entropy Correction Method for Unsteady Full Potential Flows with Strong Shocks. AIAA Paper No. 86-1768-CP.

[10]M. Hafez and D. Lovell 1983 Entropy and Vorticity Corrections for Transonic Flows. AIAA Paper 83-1926.

[11]M. Hafez, S. Osher and W. Whitlow, Jr. 1984 Improved Finite Difference Schemes for Transonic Potential Calculations. AIAA Paper 84-0092.

[12]S. Osher, M. Hafez and W. Whitlow, Jr. 1985 Entropy Condition Satisfying Approximations for the Full Potential Equation of Transonic Flow. Mathematics of Computations Vol. 44 1-29.

[13]J. O. Bridgeman, J. L. Steger and F. X. Caradonna 1982 A Conservative Finite Difference Algorithm for the Unsteady Transonic Potential Equation in Generalized Coordinates. AIAA Paper 82-1388.

[14]J. L. Steger 1978 Implicit Finite Difference Simulation of Flow about Arbitrary Two-Dimensional Geometries. AIAA Journal Vol. 16 679-686.

[15]R. L. Sorenson 1980 A Computer Program to Generate Two-Dimensional Grids about Airfoils and Other Shapes by Use of the Poisson's Equation. NASA TM 81198.

[16]R. J. Zwaan 1982 NLR 7301 Supercritical Airfoil Oscillatory Pitching and Oscillating Flap, Compendium of Unsteady Aerodynamic Measurements. AGARD Report No. 702.

[17]R. H. Landon 1982 NACA 0012. Oscillatory and Transient Pitching. Compendium of Unsteady Aerodynamic Measurements. AGARD Report No. 702.

[18]Sandford S. Davis and Gerald N. Malcom 1980 Experimental Unsteady Aerodynamics of Conventional and Supercritical Airfoils. NASA TM-81221.

[19]A. Jameson 1983 Solution of the Euler Equations for Two Dimensional Transonic Flow by a Multigrid Method. Princeton University MAE Report No. 1613.

[20]James T. Howlett and Samuel R. Bland 1987 Calculation of Viscous Effects on Transonic Flow for Oscillating Airfoils and Comparisons With Experiment. NASA TP 2731.

Figure 2. Computational cell in interior of flow field.
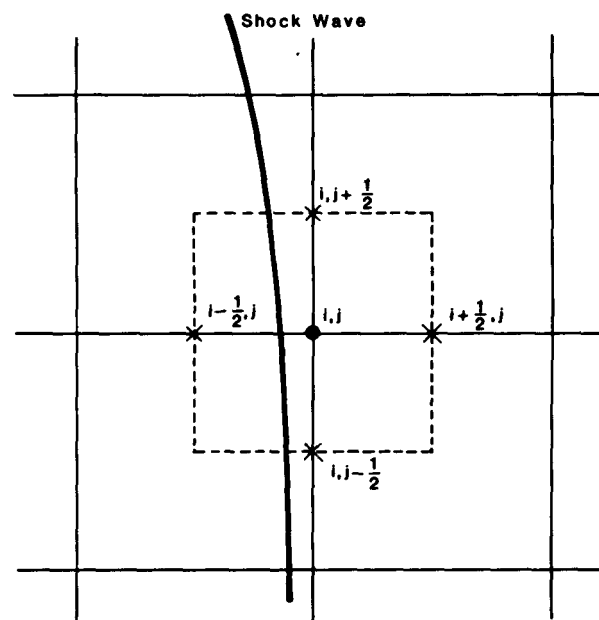
Figure 3. Computational cell at shock points.

Figure 1. Generalized coordinate system.

8
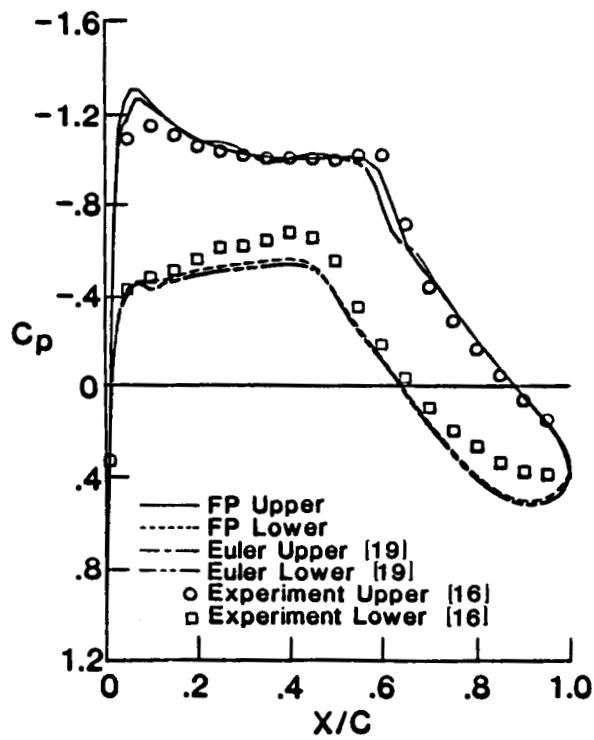
Figure 4. Steady pressures on NLR 7301 airfoil calculated using current grid, $M_\infty = 0.721$, $\alpha = -0.19°$.
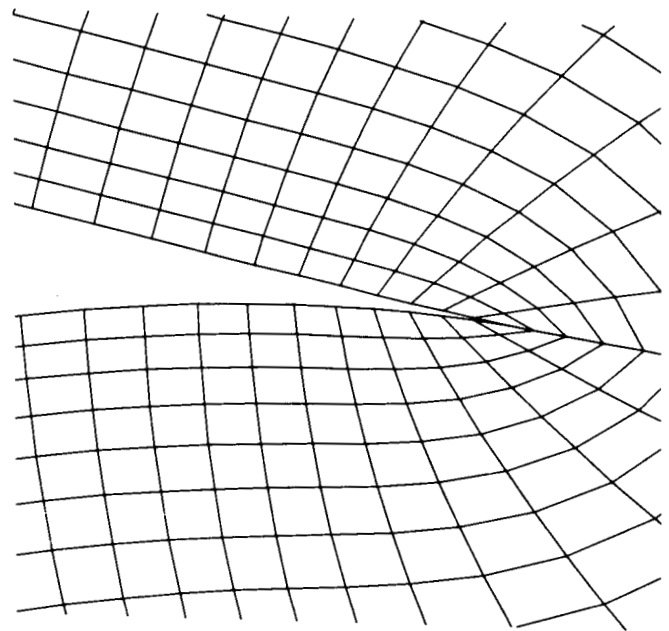
Figure 6. Original grid in trailing edge region of NLR 7301 airfoil [9].
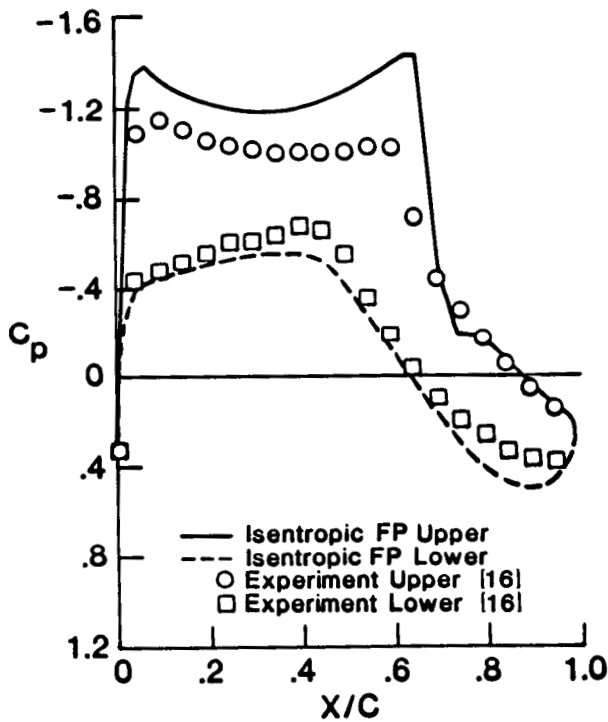
Figure 5. Steady pressures on NLR 7301 airfoil calculated using original grid, $M_\infty = 0.721$, $\alpha = -0.19°$.
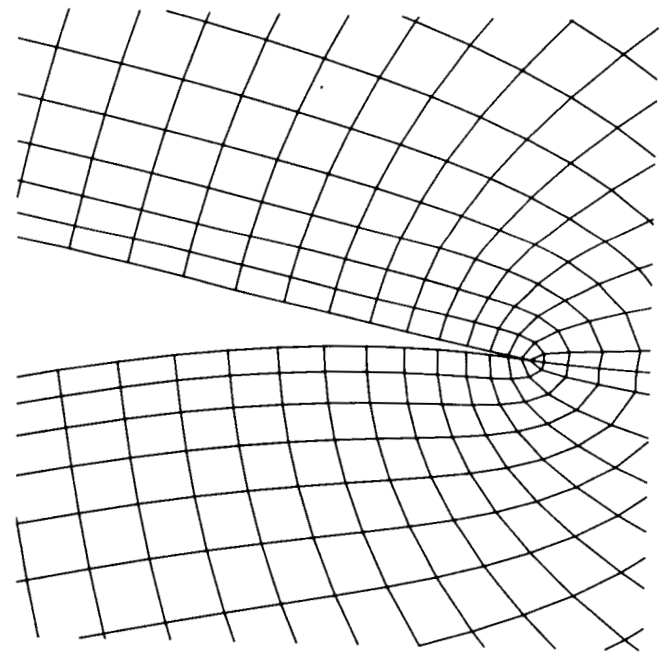
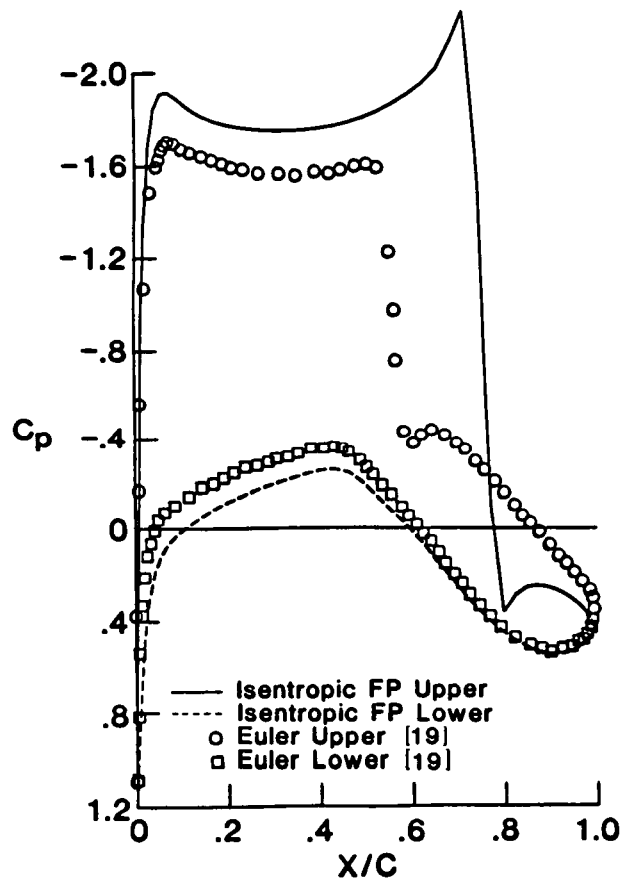Figure 7. Current grid in trailing edge region of NLR 7301 airfoil.

9

Figure 8. Isentropic potential and Euler calculated steady pressures on NLR 7301 airfoil, M_∞ = 0.7, α = 2°.
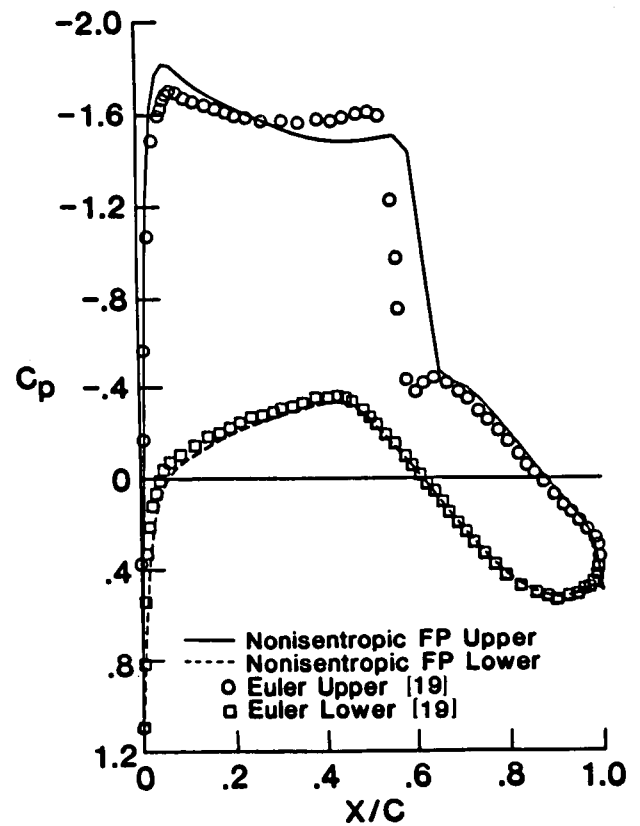
Figure 9. Nonisentropic potential and Euler calculated steady pressures on NLR 7301 airfoil, M_∞ = 0.7, α = 2°.
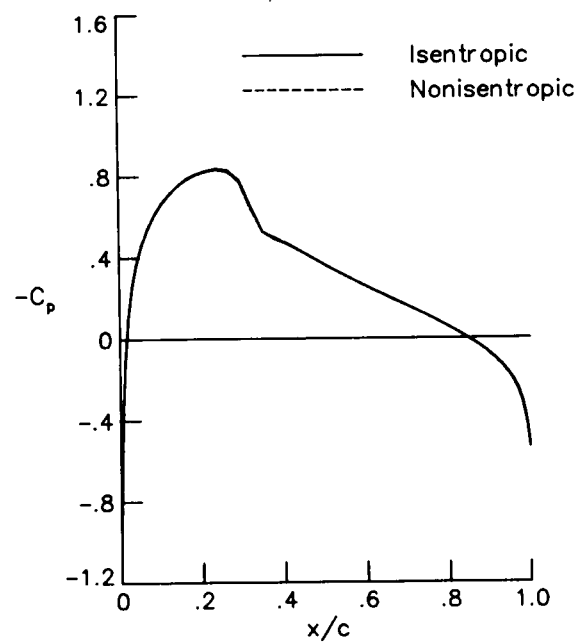
Figure 10. Steady pressures on NACA 0012 airfoil, M_∞ = 0.755, α = 0.016°.

10
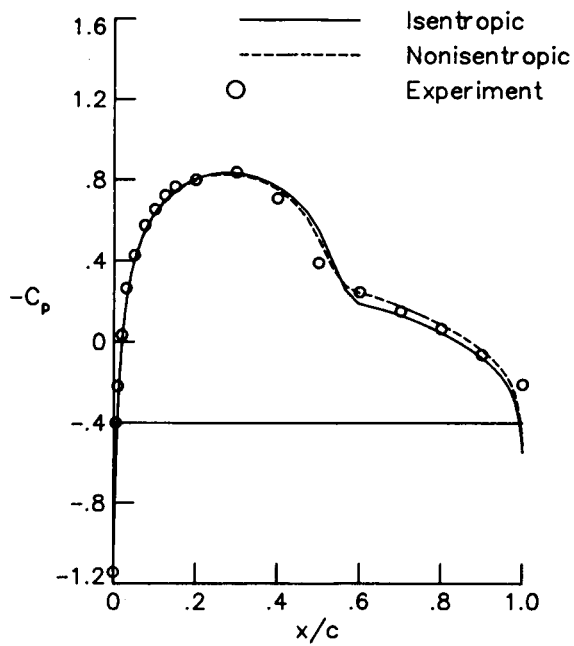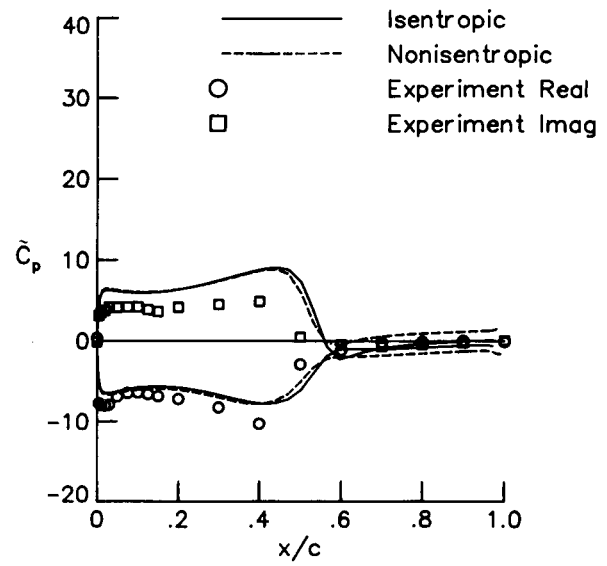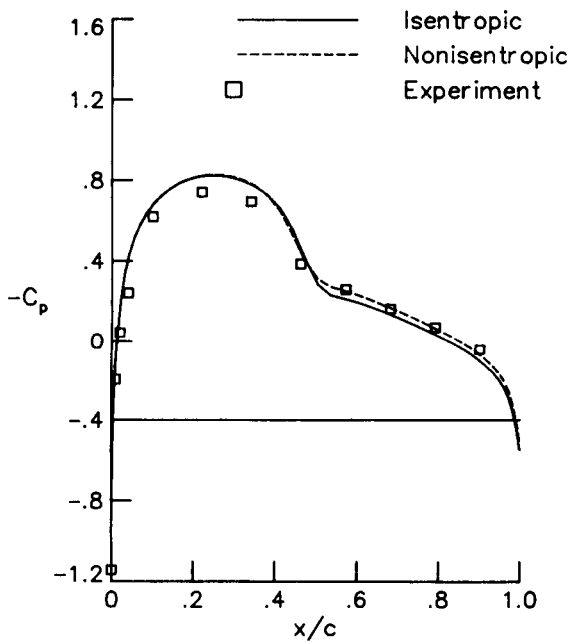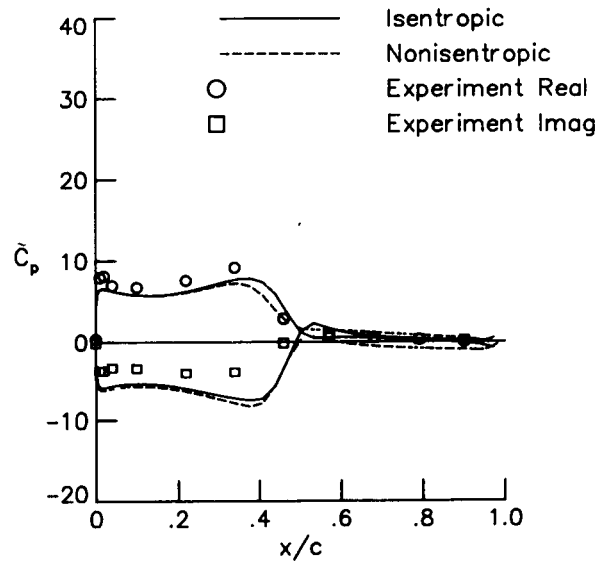
(a) Upper.

(b) Lower.

Figure 11. Mean pressures on NACA 0012 airfoil, M∞ = 0.755, α = 0.016° + 2.51° sin (kτ), k = 0.0814.

(a) Upper.

(b) Lower.

Figure 12. Unsteady pressures on NACA 0012 airfoil, M∞ = 0.755, α = 0.016° + 2.51° sin (kτ), k = 0.0814.

11
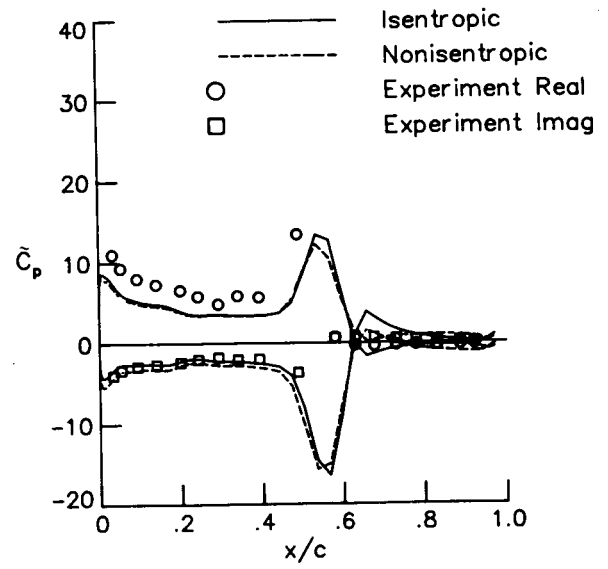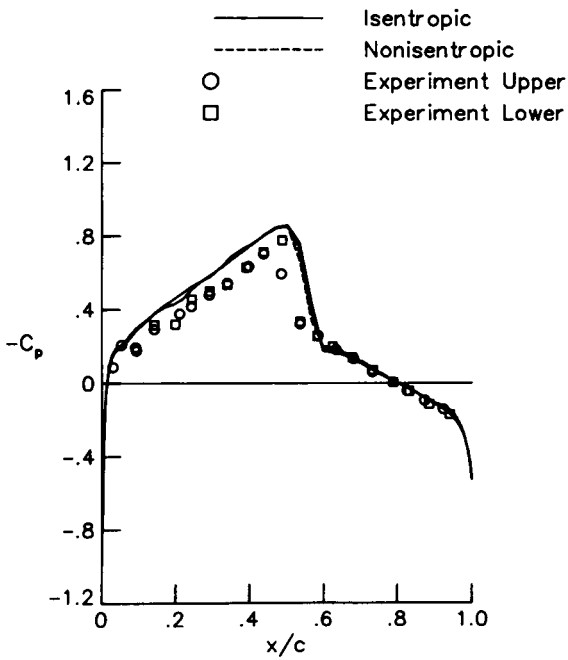
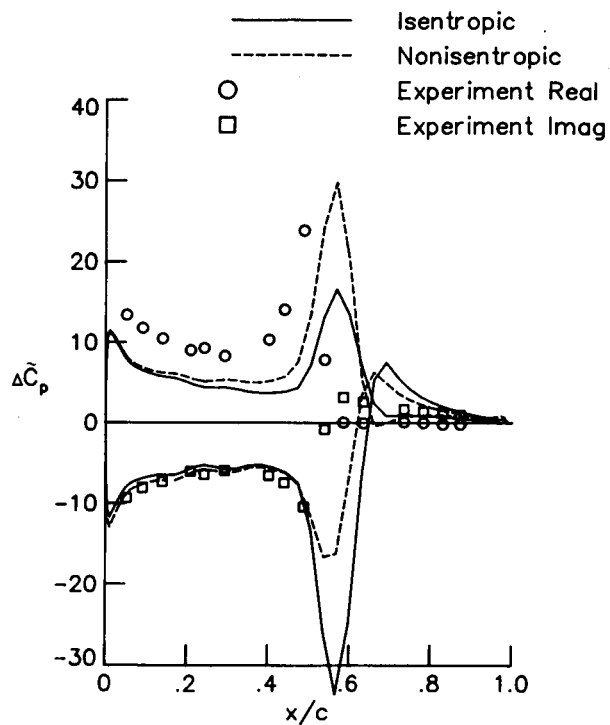Figure 13. Steady pressures on NACA 64A010A, M_∞ = 0.796, α = 0°.

(b) Lower.

(a) Upper.

Figure 14. Unsteady pressures on NACA 64A010A airfoil, M_∞ = 0.796, α = 1.02° sin (kτ), k = 0.051.
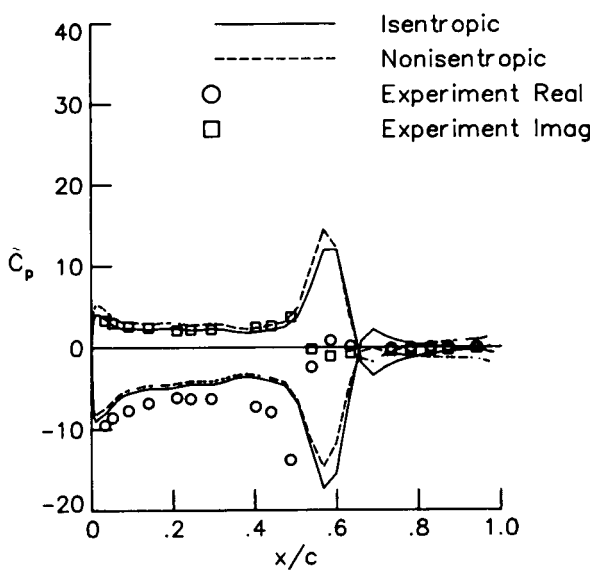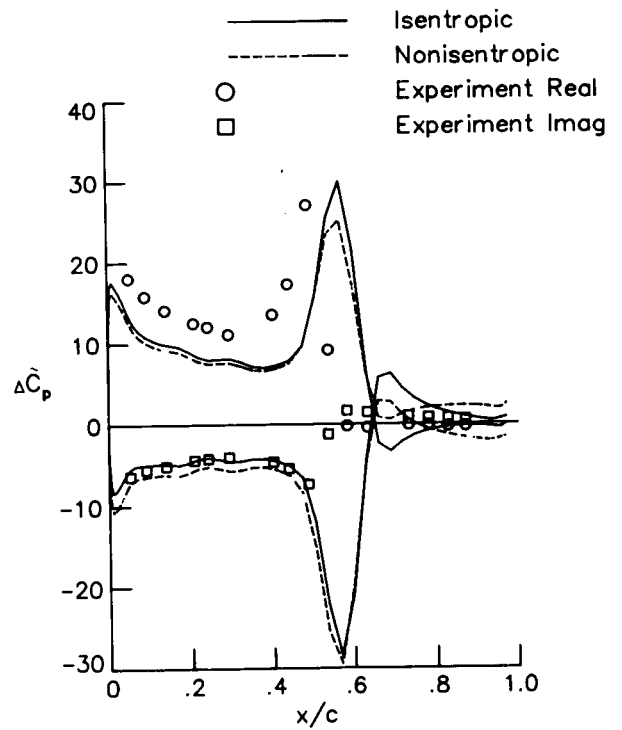
(c) Lifting.
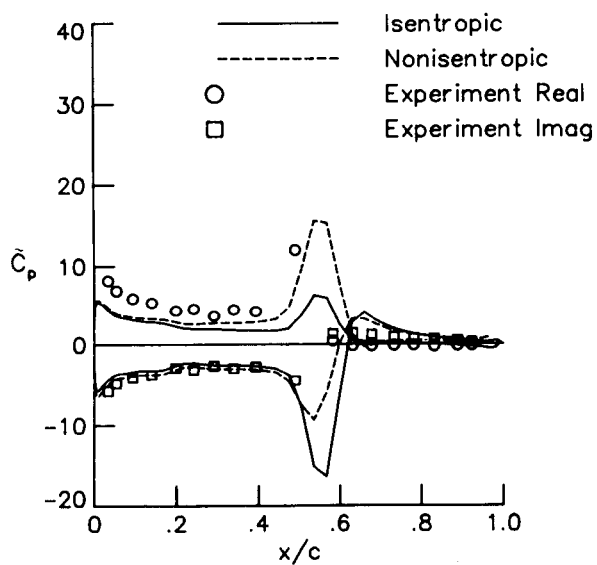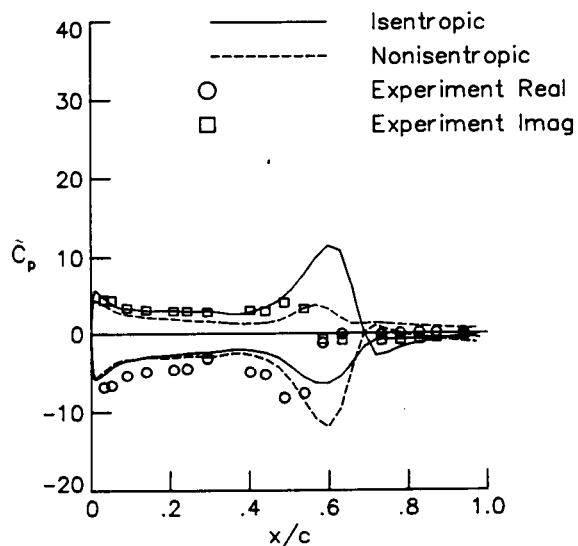
Figure 14. Concluded.
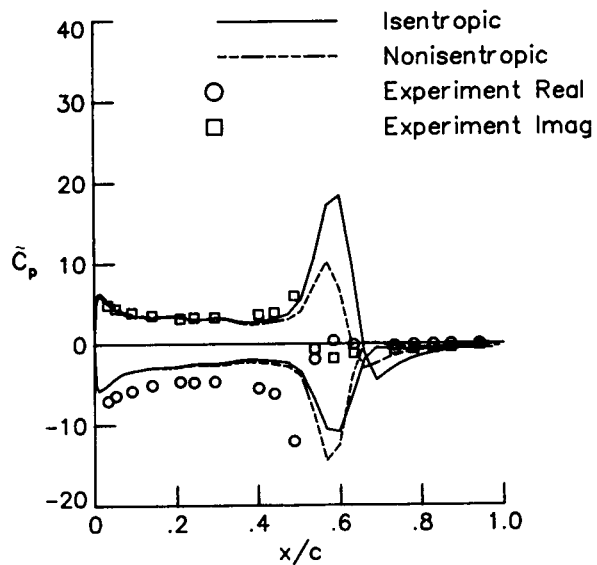
(a) Upper.

(c) Lifting.

Figure 15. Concluded.
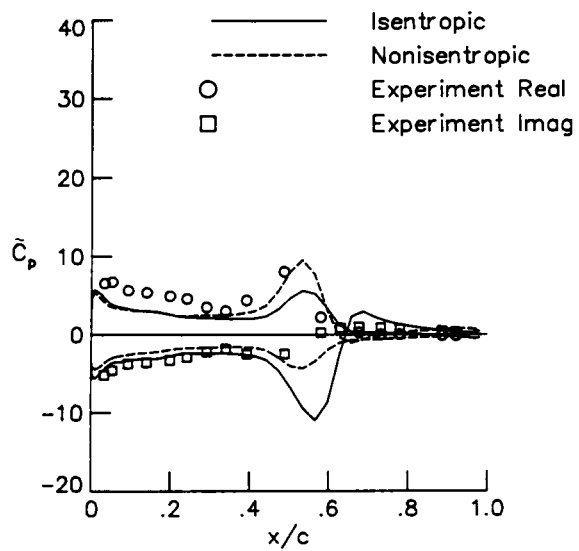
(b) Lower.

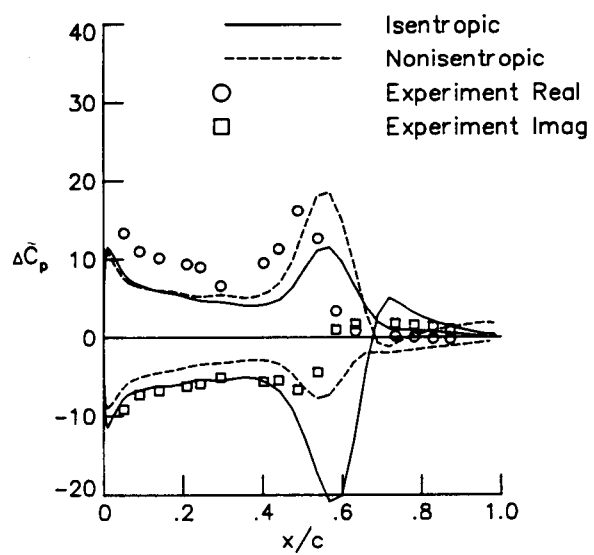(a) Upper.

Figure 15. Unsteady pressures on NACA 64A010A airfoil,
$M_\infty = 0.796$, $\alpha = 1.02°$ sin (kτ), k = 0.101.

Figure 16. Unsteady pressures on NACA 64A010A airfoil,
$M_\infty = 0.796$, $\alpha = 2°$ sin (kτ), k = 0.101.

(b) Lower.

(c) Lifting.

Figure 16. Concluded.

NASA

National Aeronautics and
Space Administration

Report Documentation Page

1. Report No.	2. Government Accession No.	3. Recipient's Catalog No.
NASA TM-100560		

4. Title and Subtitle		5. Report Date
Application of a Nonisentropic Full Potential Method to AGARD Standard Airfoils		January 1988
		6. Performing Organization Code

7. Author(s)	8. Performing Organization Report No.
Woodrow Whitlow, Jr.	
	10. Work Unit No.
	505-63-21-01

9. Performing Organization Name and Address	11. Contract or Grant No.
NASA Langley Research Center Hampton, Virginia 23665-5225	
	13. Type of Report and Period Covered

12. Sponsoring Agency Name and Address	13. Type of Report and Period Covered
National Aeronautics and Space Administration Washington, DC 20546	Technical Memorandum
	14. Sponsoring Agency Code

15. Supplementary Notes

16. Abstract

An entropy-correction method for the unsteady full potential equation is presented. The unsteady potential equation is modified to model the entropy jumps across shock waves. The conservative form of the modified equation is solved in generalized coordinates using an implicit, approximate factorization method. A flux-biasing differencing method, which generates the proper amounts of artificial viscosity in supersonic regions, is used to discretize the flow equations in space. Calculated results are presented for the NLR 7301, NACA 0012, and NACA 64A010A airfoils. Comparisons of the present method and solutions of the Euler equations are presented for the NLR 7301 airfoil, and comparisons of the present method and experimental data are presented for all three airfoils. The comparisons show that the present method more accurately models solutions of the Euler equations and experiment than does the isentropic potential formulation. In addition, it is shown that modeling shock-generated entropy extends the range of validity of the full potential method.

17. Key Words (Suggested by Author(s))	18. Distribution Statement
Unsteady Transonic Aerodynamics Full Potential Methods Entropy Corrections Nonisentropic Flows	Unclassified - Unlimited Subject Category 02

19. Security Classif. (of this report)	20. Security Classif. (of this page)	21. No. of pages	22. Price
Unclassified	Unclassified	15	A02

NASA FORM 1626 OCT 86